Defects in silicon after B^+ implantation: A study using a positron-beam technique, Rutherford backscattering, secondary neutral mass spectroscopy, and infrared absorption spectroscopy

S. Eichler, J. Gebauer, F. Börner, A. Polity, and R. Krause-Rehberg
Fachbereich Physik der Martin-Luther-Universität Halle-Wittenberg, D-06099 Halle, Saale, Germany

E. Wendler, B. Weber, and W. Wesch
Fachbereich Physik, Institut für Festkörperphysik, Friedrich-Schiller-Universität Jena, Max-Wien-Platz 1, D-07743 Jena, Germany

H. Börner
Universität Leipzig, Institut für Experimentalphysik II, Linnéstraße 5, D-04103 Leipzig, Germany
(Received 13 November 1996; revised manuscript received 21 February 1997)

The distribution of defects in Si (100), (110), and (111) after boron implantation and annealing processes was measured by means of different methods. Boron implantation was carried out at 300 K with three energies (50, 150, and 300 keV or 30, 90, and 180 keV) in multiple mode to obtain a homogeneously damaged layer. Ion fluences ranged from 10^{14} to 10^{16} B^+ cm^{-2}. The profile of vacancy-type defects was detected by variable-energy positron annihilation spectroscopy (VEPAS). The defect concentration increases proportionally to $\sqrt{\Phi}$, where Φ is the ion fluence. It was found that the line-shape parameter S of the positron-electron annihilation peak in the implanted layer increases with Φ. The divacancy $(2v)$ concentration observed by infrared absorption spectroscopy (IRAS) was nearly constant in all samples (about 1.8×10^{19} cm^{-3}). It can be concluded that divacancies are not the main vacancy-type defect and the increasing S parameter must be attributed to additional defects of larger open volume. A value $S_{\mathrm{defect}}/S_{\mathrm{bulk}}=1.048$ was fitted for the dominating defect, where $S_{2v}/S_{\mathrm{bulk}}=1.04$. Rutherford backscattering (RBS) measurements were carried out to detect the distribution of displaced lattice atoms. The defect-production rate was proportional to $\sqrt{\Phi}$ again. The concentration profiles of implanted ions were measured with sputtered neutral mass spectrometry (SNMS). In addition, Monte Carlo calculations were done with the TRIM code. The nearly homogenous defect distributions up to a depth of 1 μm found by VEPAS, TRIM, and RBS are in very good accordance. The samples were annealed up to 1150 K. It was found that the annealing behavior of vacancylike defects depends on the implantation dose and on the sample material under investigation. The divacancies are annealed at 470 K as measured by IRAS. An annealing stage of vacancy clusters at 725 K was observed in all samples by VEPAS. In Czochralski material, a decrease of the S parameter below the value of defect-free Si was observed after annealing at about 750 K. This can only be explained by the appearance of a different defect type, most likely an oxygen-vacancy complex. At high ion fluences (10^{16} B^+ cm^{-2}), an increase of the S parameter above the defect value at room temperature was observed after annealing at 700 K in a region 100 nm below the surface. This high S parameter is caused by the creation of larger vacancy clusters. These defects remain stable after annealing at 850 K. Correlated RBS and SNMS measurements were done at identically implanted samples for all annealing stages. [S0163-1829(97)03327-4]

I. INTRODUCTION

The intention for application of the ion-implantation technique is the defined doping of different impurity species into semiconductors during the fabrication process of planar devices. The major side effect of ion implantation, the radiation damage, has been studied extensively for over two decades.[1,2] The depth distribution of implanted dopants is well known. Electronic excitations and atomic collisions are the dominant energy-loss mechanisms of the incident ions. Individual atomic displacements are the primary lattice response. Lindhard, Scharff, and Schiøtt have developed the so-called LSS theory in 1963,[3] which describes the stop positions of the implanted ions with a Gaussian distribution around the projected range. More recently, Monte Carlo simulations are used to predict the primary damage after ion implantation. As an example, the TRIM code based on the binary collision approximation[4] is often used. Secondary processes such as displacements of other atoms and the formation of defect cascades are taken into account.[5] However, the behavior of implantation defects during annealing as well as diffusion effects and defect reactions are still under discussion.

Semiconductor materials have different structural, electrical, and optical properties depending mainly on dopant species and on defect structure. There are many possibilities in the near-surface region because the surface conditions have an influence on the band bending and on the resulting electric field. Therefore, it is important to investigate the same samples by several methods in the field of defect physics in semiconductors.

The variable-energy positron annihilation spectroscopy (VEPAS) has turned out to be a very useful tool to detect open-volume defects because of its nondestructiveness and

 © 1997 The American Physical Society

high sensitivity.[6,2] Sputtered neutral mass spectrometry (SNMS) and Rutherford backscattering spectroscopy (RBS) are often used to detect the dopant distribution and the behavior of displaced lattice atoms, respectively. We observed the annealing of divacancies by infrared absorption spectroscopy (IRAS).

In this work we investigated the damage of ion implantation in the micrometer depth region. All methods used for the defect detection, VEPAS, RBS, SNMS, and IRAS are especially sensitive in this range.

II. EXPERIMENT

A. Sample material and ion implantation

Measurements were carried out at different sample series to investigate dependences on implantation fluences and directions. All samples were implanted with B^+ ions at 300 K. We used p-type $[B]$ Czochralski silicon (10–30 Ω cm) with $\langle 111\rangle$, $\langle 110\rangle$, and $\langle 100\rangle$ orientations and undoped silicon to investigate the annealing behavior and dependences of ion-beam-induced damage on the implantation direction and implantation fluence, respectively. To discuss the influence of oxygen concentration, we irradiated Czochralski Si (n-type $[P]$, $\rho = 0.6\ \Omega$ cm) and floating zone (FZ) material (n-type $[P]$, $\rho = 0.5\ \Omega$ cm) under similar conditions. The oxygen concentration of all Czochralski samples was about $1\times 10^{18}\ \mathrm{cm}^{-3}$, whereas this concentration was 1×10^{16} for FZ material. All implantations were done in the 7° off-axis direction, which is typically used to avoid channeling effects. In order to get sufficiently thick layers with an almost homogeneous damage profile, B^+ ions were subsequently implanted with energies of 300, 150, and 50 keV. For the 300-keV implantation the ion fluence was varied between 1×10^{14} and $2\times 10^{16}\ \mathrm{cm}^{-2}$. TRIM simulations were carried out with minimal 5000 ions to calculate the fluence ratios for the different implantation energies in order to obtain a homogeneous damage profile. We found that the best ratios are 2:1:0.45 at 300, 150, and 50 keV, respectively. To identify the samples in the subsequent discussion, the ion fluence for the largest implantation energy is indicated as Φ. The samples for the annealing experiments were implanted with 30, 90, and 180 keV in a similar mode. Homogeneous damage profiles allow an easier interpretation of experimental data for the VEPAS measurements (compare Fig. 3) because of its limited depth resolution. The samples were annealed *in situ* at a pressure of 10^{-6} Pa during the positron experiment. The annealing of samples for RBS, SNMS, and IRAS were performed in an argon atmosphere at a pressure of 10^{-2} Pa.

B. Slow positron beam

The variable-energy positron beam was produced by a 1.8 GBq β^+ source of ^{22}Na assembled in transmission with a 5-μm polycrystalline tungsten moderator, transported by some solenoids. The beam having a diameter of 5 mm and an intensity of $5\times 10^5\ e^+/\mathrm{s}$ was made to strike the sample. The samples were mounted in an UHV chamber at a temperature controlled sample holder (90–1200 K). The γ annihilation spectrum was recorded with a high-purity Ge detector having an energy resolution of 1.9 keV at 1.2 MeV. The data were acquired with a digitally stabilized multichannel-analyzer system. The Doppler broadening of the 511-keV γ-ray peak was measured at room temperature as a function of incident positron energy from 0.1 to 39 keV. 8×10^5 counts were collected in the 511-keV annihilation line at each incident energy.

C. RBS measurements

Rutherford backscattering measurements were performed at 100 and 239 K using 1.4-MeV He^+ ions and a backscattering angle of 177°. For the analysis, the difference in minimum yield $\Delta\chi_{\min}$ was determined, which is given by

$$\Delta\chi_{\min} = \frac{Y_{\mathrm{al}}^{\mathrm{imp}} - Y_{\mathrm{al}}^{\mathrm{perf}}}{Y_{\mathrm{ra}}}, \tag{1}$$

where $Y_{\mathrm{al}}^{\mathrm{imp}}, Y_{\mathrm{al}}^{\mathrm{perf}}$ are the backscattering yields in the aligned direction for the implanted and the perfect crystal, respectively. Y_{ra} is the backscattering yield in random direction. From the $\Delta\chi_{\min}$ spectra measured at the two different temperatures, the relative concentration n_{DA} of displaced lattice atoms and their mean displacement distance r_a perpendicular to the axis of incidence were determined in the framework of the discontinuous model of dechanneling[7,8] using the computer code DICADA.[9] The existence of uncorrelated displaced lattice atoms in the damaged layers was assumed and the thermal vibration of these atoms was taken into account.

D. SNMS and IR absorption

SNMS investigations were performed with the device INA 3 (Leybold/Specs). The samples were bombarded by positive ions extracted from a low-pressure high-frequency plasma (Kr^+). The sputtered neutral atoms were post-ionized by electron impact in the plasma and mass-selectively detected by a quadrupole mass filter. A standard plasma pressure $p(\mathrm{Kr})$ of about 1.9×10^{-3} Torr, a rf power of 150 W, and a Helmholtz coil current of 5.2 A were employed. A constant dc bombardment voltage of 550 V was applied to the sample. The depth of the sputtered crater in the sample was measured by a surface profiler (DEKTAK 3030).

The IR investigations were performed on polished samples using a Lambda 19 (Perkin Elmer). The absorption coefficient shows an exponential tail in the near-edge region, which is superimposed by the divacancy absorption band (0.68 eV). The absorption exponent ε of the implanted Si layers was determined in the frequency range $0.5\ \mathrm{eV} \leqslant \hbar\omega \leqslant 1.15\ \mathrm{eV}$ by conventional transmission measurements. Assuming a homogeneously implanted layer, the absolute absorption coefficient k can be calculated dividing ε by the layer thickness d obtained from the positron experiment. The exponential tail is interpolated and subtracted in the region of the absorption band. The divacancy concentration is proportional to the intensity of the absorption band.[10]

III. DEFECT PROFILING USING THE POSITRON BEAM TECHNIQUE

A. Positron implantation and diffusion

When positrons enter a solid, at first a rapid energy loss happens, where positrons reach thermal energies. An ap-

proximation for the resulting positron implantation profile is the Makhov distribution, suggested by Valkealahti and Nieminen,[11]

$$P(E,z)=\frac{mz^{m-1}}{z_0^m}\exp\left[-\left(\frac{z}{z_0}\right)^m\right], \tag{2}$$

where $m=2$ and z_0 is related to the mean implantation depth $\bar{z}$ by

$$z_0=\bar{z}/\Gamma(1/m+1). \tag{3}$$

Γ means the Gamman function. The mean depth $\bar{z}$ (Å) is obtained by

$$\bar{z}=\frac{A}{\rho}E^n, \tag{4}$$

where ρ ($\mathrm{g\,cm^{-3}}$) is the mass density. $A=2.75$ $\mu\mathrm{g\,cm^{-2}\,keV^{-n}}$ and $n=1.7$ are empirical parameters for silicon.[12,13] After thermalization, positrons will diffuse in the solid until they annihilate. The diffusion can be described by the one-dimensional time-independent diffusion equation

$$0=D_+\frac{d^2}{dz^2}c(z)-\frac{d}{dz}[v_d(z)c(z)]-\lambda_{\mathrm{eff}}c(z)+p(z), \tag{5}$$

with $v_d(z)=\mu_+\varepsilon(z)$. $c(z)$ is the positron density, D_+ the positron diffusion constant, μ_+ the positron mobility related to the diffusion constant by the Nernst-Einstein equation, $\varepsilon(z)$ the local electric field in the z direction, $p(z)$ the positron stopping rate at depth z, and λ_{eff} the effective positron annihilation rate. In this work, we will neglect the influence of electric fields on positron diffusion. This is reasonable since there is only a weak surface band bending due to the pinned midgap position of the Fermi level. This is a result of the high concentration of implantation defects in all as-implanted samples. The diffusion coefficient for positrons in bulk silicon at 300 K is $D_+=2.7$ $\mathrm{cm^2/s}$.[14] Using a positron lifetime $\tau_b=1/\lambda_b=218$ ps in defect-free silicon,[2] the positron diffusion length $L_+=\sqrt{D_+/\lambda_b}$ is 245 nm.[14] λ_b is called the bulk annihilation rate for annihilation in the perfect crystal. Negatively charged and neutral open volume defects are attractive traps for positrons. The effective positron annihilation rate is then given by

$$\lambda_{\mathrm{eff}}=\lambda_b+\mu_t n_t, \tag{6}$$

where μ_t (t abbreviates trap) is the defect-specific trapping coefficient and n_t is the defect density. The product $\mu_t n_t=\kappa_t$ is the defect trapping rate for positron capture into defects. In the case of a homogeneous defect distribution, L_+ is replaced by the effective diffusion length $L_{+,\mathrm{eff}}=\sqrt{D_+/\lambda_{\mathrm{eff}}}$, where a small $L_{+,\mathrm{eff}}$ means a high defect density. $L_{+,\mathrm{eff}}$ can be extracted from the experimental data by the program VEPFIT (Ref. 15) (see below). The defect trapping rate κ_t and, with a known trapping coefficient μ_t, the defect density n_t are given by

$$\kappa_t=\mu_t n_t=\lambda_b\left[\left(\frac{L_+}{L_{+,\mathrm{eff}}}\right)^2-1\right]. \tag{7}$$

Positrons may also annihilate at the sample surface. Additionally, positrons can be reemitted from clean surfaces, either as bound with an electron, as positronium, or in a free state. However, for the silicon oxide covered samples used in this study the reemission probability can be neglected.[6]

B. Annihilation parameters

The momentum of the annihilating electrons causes a Doppler broadening of the emitted γ-radiation line. For this reason, the shape of the 511-keV annihilation line is sensitive to the local electronic environment in the solid and will differ between annihilations in defects and in the perfect lattice. Usually, the shape of the 511-keV line is analyzed by using the line-shape parameters S and W. The S parameter is defined as the ratio between the number of counts in the center (511 ± 0.8 keV) to the total peak area, whereas the W parameter is defined as the ratio between the wing area ($\geqslant 511+2.8$ keV) to the total peak area. Every kind of defect yields a characteristic S and W value. In general, in the presence of open-volume defects, the S parameter is higher than the bulk value, whereas the W parameter is lower. A measured S parameter (similar also W) is a linear combination of the specific S parameters for different annihilation sites, such as

$$S=f_{\mathrm{bulk}}S_{\mathrm{bulk}}+f_sS_s+\sum f_{t,j}S_{t,j}, \tag{8}$$

where the f_i ($\Sigma f_i=1$) are the fractions for annihilation in the bulk, at the surface, and in defect type j. So a change in S can be caused by a change of the defect type or by a change of the defect concentration. By using S and W, one can define a R_b parameter, which depends only on the defect type,[16,17] but is independent of the defect concentration, as

$$R_b=|(S-S_{\mathrm{bulk}})/(W-W_{\mathrm{bulk}})|. \tag{9}$$

This is valid if only one defect type is present, which is surely not true in the case of ion implantation. But one can redefine a R that is independent of the defect concentration too, in the case of saturation trapping in two different defect types. Then S is written as

$$S=f_1S_1+f_2S_2, \tag{10}$$

where S_i is the S parameter for annihilation in defect i and $f_1+f_2=1$. Then the changes in S due to a change in the defect concentration can be written as

$$S-S_2=f_1(S_1-S_2). \tag{11}$$

An equivalent equation can be found for the W parameter. Then R can be defined by dividing both equations

$$R=\left|\frac{S-S_2}{W-W_2}\right|=\left|\frac{S_1-S_2}{W_1-W_2}\right|. \tag{12}$$

With that, R depends only on the defect types involved and not on the defect concentrations. This definition is similar to Eq. (9), but S_{bulk} is replaced by a typical defect S parameter (see the discussion in Sec. IV A 1).

For data analysis in this work, we used the fitting and modeling program VEPFIT (for details see Ref. 15). The pro-

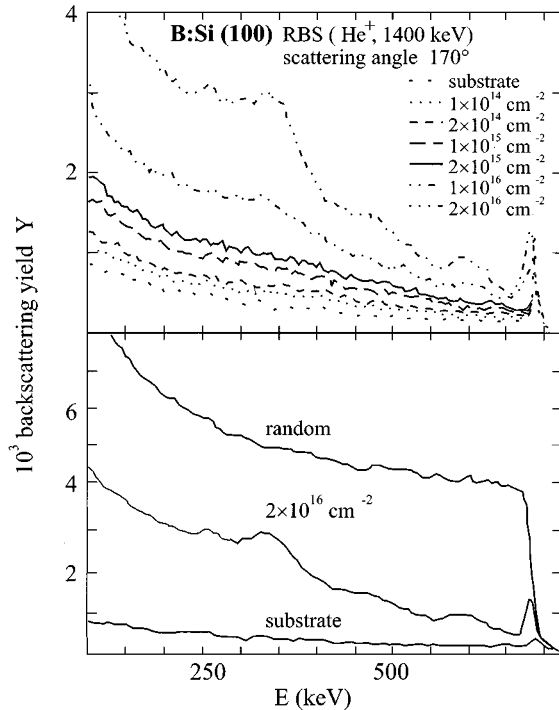

FIG. 1. RBS spectra of Si(100) implanted with different boron fluences (upper part) and a comparison (lower part) between the RBS spectra for the largest implantation fluence and a random spectra, which is typical for amorphous material.

gram solves the diffusion equation (5) for a given layer structure. Equation (8) is fitted to the experimental S parameter data. S_s is obtained from the S parameter data at low incident energies, when nearly all positrons reach the surface. S_s is usually different from S_{bulk} and depends on the surface conditions. S_{bulk} is obtained from measurements at high incident energies or from reference samples, when nearly all positrons annihilate in the defect-free bulk beyond the implanted layer. Then the fit results are the positron diffusion lengths, the thicknesses, and the S parameters of the different layers. The W and R parameter data are used for additional information, such as changes in the defect type.

IV. RESULTS AND DISCUSSION

A. As-implanted state

1. Implantation with different fluences

As an example for the damage evolution as visible by RBS, Fig. 1 shows the energy spectra of 1.4-MeV He^+ ions backscattered on B^+-implanted ⟨100⟩ silicon. For ion fluences $\Phi \leqslant 1\times10^{16}\,\mathrm{cm}^{-2}$ the backscattering spectra are mainly characterized by dechanneling of the analyzing ions, suggesting the existence of point defects and point defect complexes, the concentration of which increases with increasing ion fluence (see upper part of Fig. 1). After implantation of $2\times10^{16}\,B^+\,\mathrm{cm}^{-2}$ the occurrence of peaks in the spectrum indicates a distinct contribution of direct backscattered He^+ ions to the measured yield. Therefore, defect clusters are to be expected, which are connected to the existence of displaced lattice atoms having large displacement distances from the atomic rows. However, comparing the back-

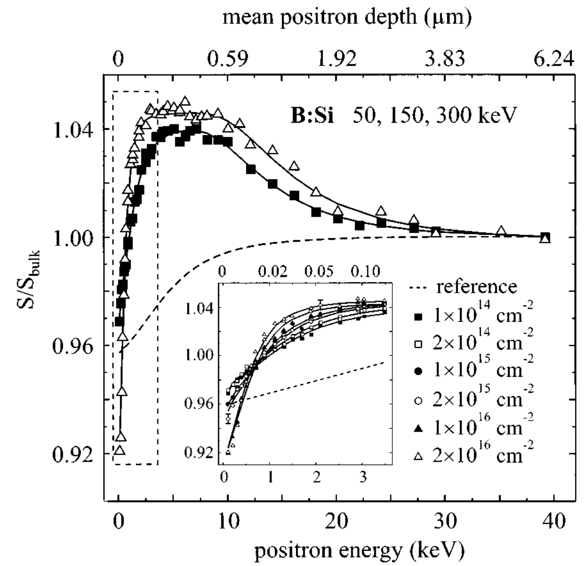

FIG. 2. $S(E)$ curves of undoped Czochralski Si implanted with 2×10^{16} and $1\times10^{14}\,\mathrm{cm}^{-2}$ boron ions at an off-normal orientation mode are shown exemplarily. The different slopes of the first part of all curves can be seen in the inset for a more extended fluence series. The lines are best fits to the positron diffusion equation by VEPFIT.

scattering spectrum for $\Phi = 2\times10^{16}\,B^+\,\mathrm{cm}^{-2}$ with the random spectrum (see lower part of Fig. 1) it is obvious that the total damage level is still low and the implanted layer contains no amorphous zones.

The data of slow positron measurements shown in Fig. 2 exhibit the dependence of implantation damage on fluence. There are only two annihilation sites for the positrons for the nonimplanted sample (reference). First, at low incident energies the measured S parameter is characteristic for the surface caused by the thin natural oxide layer. Second, at high energies (>15 keV) all positrons annihilate in the defect-free silicon. In the energy range between 0 and 15 keV, more or less positrons diffuse back to the surface. Here the course of the mixed S parameter [Eq. (8)] shows a characteristic behavior for the positron diffusion length in silicon (245 nm). Furthermore, the S parameter curves (shown in Fig. 2) are typical for damaged layers in silicon produced by ion implantation.[2] The low surface S parameter caused by a thin natural oxide layer at the surface increases at larger implantation fluences; this means that the microstructure of the oxide layer changes during implantation and is a function of fluence. A similar behavior was found by Uedono et al. at γ-irradiated SiO_2.[18] However, these differences are not important in the following context, as they merely reflect different surface conditions of the samples. The important differences are the slopes of the curves to the S parameter plateau between 2- and 10-keV positron energy, which corresponds to the change of the effective positron diffusion length. It can be assumed that even for the lowest fluence the trapping in the damaged layer is saturated, i.e., the fraction of trapped positrons f_t is nearly 1. This fraction can be calculated by

$$f_t = \frac{\kappa_t}{\kappa_t + \lambda_b}, \tag{13}$$

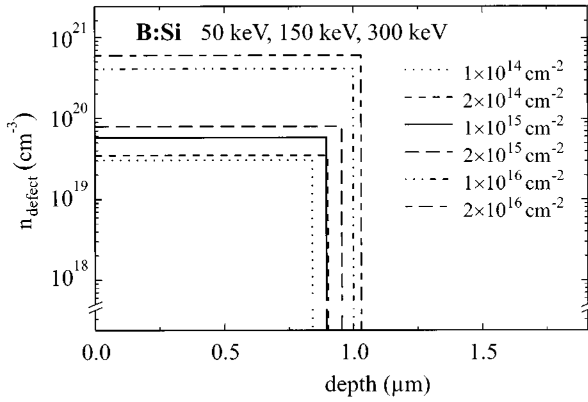

FIG. 3. Resulting box profiles of the VEPFIT fit are shown for different implantation fluences. The thickness of the damaged layer and the defect concentration increase with higher fluence.

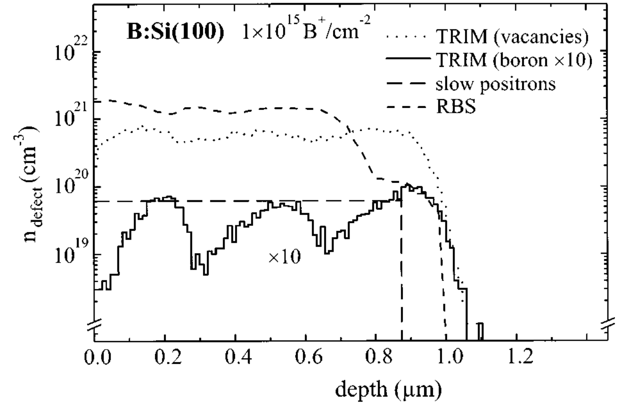

FIG. 4. Comparison of defect profiles determined by TRIM, RBS, and VEPAS exemplarily shown for the sample implanted with 1×10^{15} B^+cm^{-2}.

with a known trapping rate κ_t [see Eq. (7)]. This means that the typical defect S parameter can be determined directly from the plateau value of $S(E)$ curves, which also was verified by the VEPFIT fit. The common high-energy asymptote represents the characteristic S parameter of undamaged bulk material (S_{bulk}). It indicates that above 30 keV most of the positrons are implanted deep enough to annihilate beyond the disordered layer.

As known from the TRIM results, the defect profiles can be approximated with boxes of homogeneous defect density. Under these conditions, the effective positron diffusion length $L_{+,\mathrm{eff}}$ and the depth of the damaged layer are the only free nonlinear parameters of the fitting procedure in VEPFIT. The defect concentration can be deduced according to Eq. (7). The exact positron trapping coefficients for all different defects are unknown. It is usual to calculate the defect concentration of open volume defects (up to small vacancy cluster) with the positron trapping coefficient for divacancies ($\mu_{2v} = 8 \times 10^{14}$ s^{-1}).[19] This procedure may be erroneous, i.e., the defect densities would be overestimated. However, the error should be not larger than a factor n, where n corresponds to the difference number of vacancies in a small vacancy cluster to the divacancy. This is due to the following arguments: (a) Defects beside divacancies are small vacancy clusters (see discussion below) and (b) positron trapping coefficients are proportional to the number of vacancies of small clusters.[20] The resulting concentration profiles $n_{\mathrm{defect}}(z)$ are plotted in Fig. 3 for different ion fluences. It can be seen that the concentration of vacancylike defects increases with larger ion fluences. It is obvious from Fig. 3 that the thickness of the damaged layer increases also with higher implantation fluence. This could be understood as an artifact of fitting procedure because we assumed box profiles. In contrast, Uedono *et al.*[21] found a shift of the damage peak towards the surface in boron-implanted silicon (80 keV) with increasing fluences between 5×10^{12} and 5×10^{15} cm^{-2}. This was concluded from the corresponding shift of the maximum of $S(E)$ curves to the surface, but not by a fitting procedure. The results of Uedono *et al.* are possibly caused by the special implantation conditions through a 43-nm-thick oxide layer. Especially at low defect concentrations, i.e., at low trapping rates, there is a strong superimposition of positron implantation and diffusion and thus a quantitative evaluation is necessary. The comparison of the calculated defect profiles by the different methods (TRIM, RBS, and VEPAS) shows that the TRIM calculation leads to slightly deeper defect profiles (see Fig. 4). A summary of the results is given in Fig. 5, in which the defect density n_{defect} obtained by VEPAS, the difference in minimum yield $\Delta_{\chi\,\mathrm{min}}$ from RBS, and the concentration of divacancies from the IR absorption band around $\hbar\omega = 0.68$ eV are depicted versus the ion fluence Φ. n_{defect} is a measure of the total concentration of open-volume defects in general and $\Delta\chi_{\mathrm{min}}$ (here taken at a depth of 1.2 μm) comprises information about the total damage concentration of implanted layers. Both quantities follow a square-root dependence on the ion fluence Φ (see Fig. 5). A similar behavior in the same fluence range was found by Sealy *et al.* for the integral strain measured by x-ray diffraction in 50-keV and 1-MeV boron-implanted silicon.[22] Such a

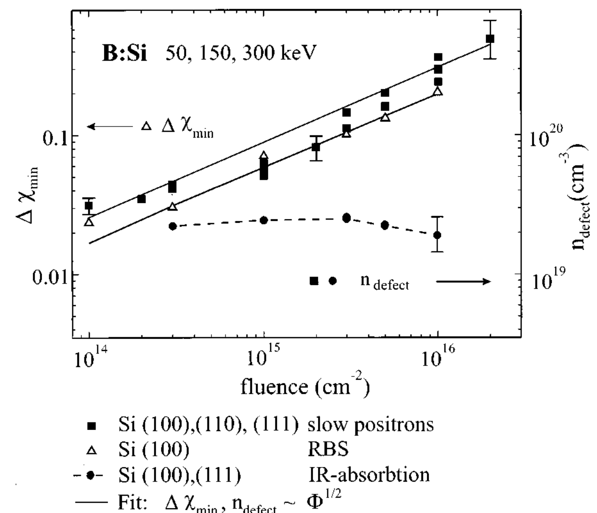

FIG. 5. Mean density of open-volume defects after boron implantation, concentration of divacancies, and difference of minimum yield as a function of fluence calculated from results by slow positrons, IR absorption, and RBS, respectively. The concentrations of open-volume defects and displaced Si atoms are proportional to the square root of fluence (straight line), whereas the divacancy concentration is nearly constant (dotted line).

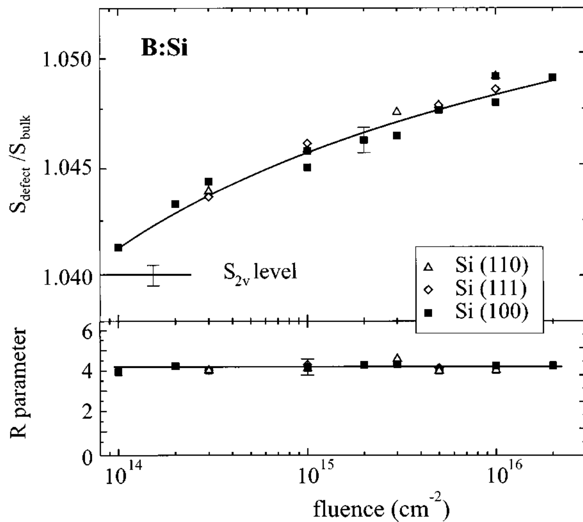

FIG. 6. S parameter and defect-specific R parameter in the damaged layer as a function of implantation fluence. The R parameter was determined with respect to the annihilation parameter of divacancies [$S_{2v}/S_{bulk}=1.04$ (Refs. 25 and 26) and $W_{2v}/W_{bulk}=0.935$ (Refs. 25 and 40)]. For details see the text.

square-root dependence is typical for defect evolution via homogeneous nucleation. This means that the primarily produced defect cascades containing single-point defects are able to dissociate due to thermally or ionizationally stimulated processes. If these point defects are mobile at the present temperature, a homogeneous concentration of vacancies and interstitials will be generated and temporary and stable defect complexes are created by the aggregation of these randomly distributed mobile point defects.[23]

Figure 5 illustrates that the concentration of divacancies remains almost constant up to ion fluences of 3×10^{15} cm^{-2}, i.e., its concentration is saturated at the applied ion fluences.[24,10] For higher fluences the divacancy concentration decreases weakly, indicating that they are suppressed above a critical density. This observation as well as the measured maximum value of 3×10^{19} cm^{-3} agree well with earlier results of Stein *et al.*[10] Comparing the concentration of divacancies with that of all open-volume defects n_{defect} as determined by VEPAS, one finds that at least one larger open-volume defect type must exist beside divacancies for B^+ implantation with fluences larger than 1×10^{14} cm^{-2}. For increased fluences n_{defect} still increases, whereas the number of divacancies is already saturated. Information about the structure of the defect complexes can be obtained from the S parameter. Figure 2 already shows that this value varies with the ion fluence. Such an increase of the S parameter cannot be explained by an increasing concentration of only one defect type for the saturated trapping state, thus pointing to the existence of at least two types of open-volume defects. In order to analyze this behavior more in detail, the S parameter in the damaged layer and the defect specific R parameter are plotted versus the ion fluence in Fig. 6. As derived in Sec. III B, the R parameter remains constant in the case of saturated trapping into two types of defects. A significant change of the R parameter is expected when a third defect type is detectable or when the assumption of saturated trapping is no longer valid. Since saturated trapping is already

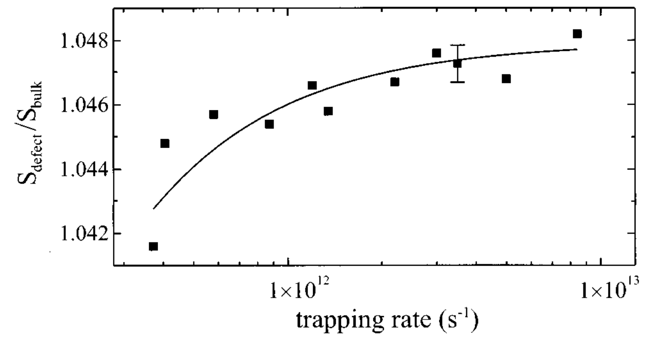

FIG. 7. Fit of the S parameter according to Eq. (16).

achieved at the lowest implantation fluence and the R parameter remains constant over the entire fluence range, one has to conclude that no further defect type becomes visible by slow positrons. On the other hand, the S parameter in the damaged layer increases continuously with increasing ion fluence. The published value $S_{2v}/S_{bulk}=1.035$ for divacancies[25,26] was corrected by Simpson to $S_{2v}/S_{bulk}=1.04$.[27] However, an increasing S parameter does not mean an increasing concentration of only one existing defect because there is saturated trapping and the constant R parameter shows that there is no change in the type of defects. Consequently, from both the constant value of the R parameter and the increasing S parameter as a function of the ion fluence, it can be concluded that divacancies and one additional larger open-volume defect type exist in the implanted-silicon layer. Assuming complete trapping in two different defects (divacancies and vacancy clusters), the S parameter in the defect-rich layer can be calculated as

$$S_{defect}=f_{2v}S_{2v}+f_{cl}S_{cl} \tag{14}$$

with

$$1=f_{2v}+f_{cl}. \tag{15}$$

The fractions f_{2v} and f_{cl} can be determined from the divacancy concentration n_{2v} measured by infrared absorption and the trapping rate κ of both defect types is obtained from positron measurements according to Eq. (7). It is

$$S_{defect}=\frac{\mu_{2v}n_{2v}}{\kappa}S_{2v}+\frac{\kappa-\mu_{2v}n_{2v}}{\kappa}S_{cl}. \tag{16}$$

In Fig. 7 the points represent the measured values of S_{defect}/S_{bulk} (corresponding to the averaged plateau values in Fig. 2) and the full line is the best fit with Eq. (16) using an appropriate value of S_{cl}. The errors of the evaluation procedure are mainly caused by the uncertainty of IR absorption results (10%) and by the value of the trapping coefficient μ_{2v} in the positron experiment. As can be seen, on the basis of this analysis a satisfactory description of the experimental results can be given, thus supporting our assumption of two different kinds of open-volume defects. The obtained value of S_{cl}/S_{bulk} amounts to 1.048 ± 0.001. A similar value was also determined by Nielsen *et al.* for 5 MeV, 1×10^{14} Si^+ cm^{-2} implanted Czochralski Si and it is assumed that this value is connected to the existence of small vacancy agglomerates.[28] Electron paramagnetic resonance investiga-

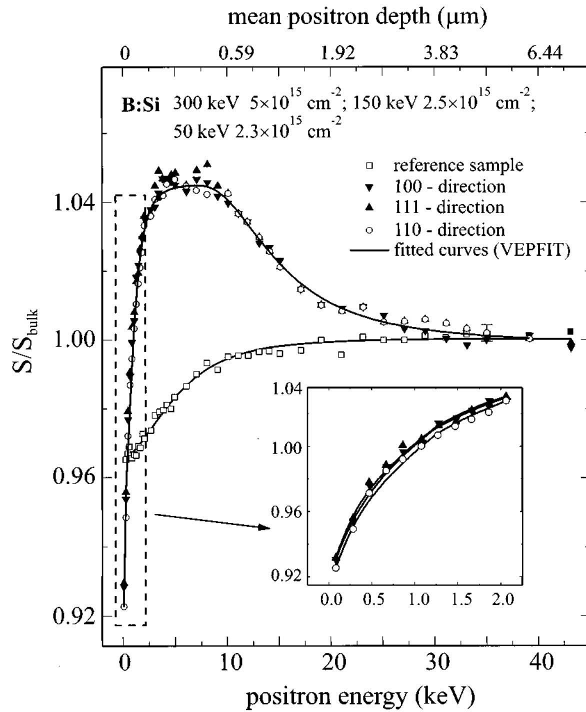

FIG. 8. $S(E)$ curves for p-type Czochralski Si (10–30 Ω cm) implanted with 5×10^{15} B$^+$ cm^{-2} in the ⟨111⟩, ⟨110⟩, and ⟨100⟩ directions. The dashed box is magnified and shown in the inset. The slopes of the curves are nearly the same.

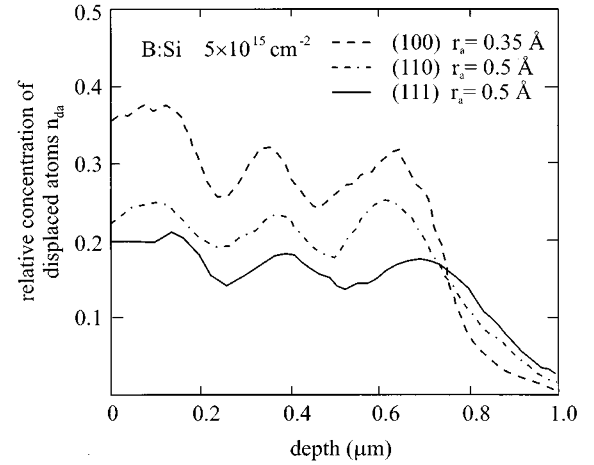

FIG. 9. Defect profiles obtained from RBS of p-type Czochralski Si (10–20 Ω cm) implanted with 5×10^{15} B$^+$ cm^{-2} in the directions ⟨111⟩, ⟨110⟩, and ⟨100⟩. The triple structure of the profiles is a result of the multiple implantation with three energies. The profiles are different from each other. In addition, the calculated displacement distances r_a are different.

tions by Sealy *et al.*[22] show for similarly irradiated samples the existence of Si $P3$ centers, which were identified as planar silicon tetravacancies,[29] and of Σ centers associated with vacancy clusters.[30] This agreement implies that small vacancy clusters were also measured. The S parameter of divacancies was verified in the free fit ($S_{2v}=1.0403$ and $S_{\mathrm{cl}}=1.0478$ were free parameters).

2. Dependence on implantation direction

We investigated the dependence of implantation damage on the substrate directions (⟨111⟩, ⟨110⟩, and ⟨100⟩) in the fluence range 10^{14}–10^{16} B$^+$ cm^{-2}. Measured values of S parameters versus positron energy are shown in Fig. 8 for an as-grown sample and three samples implanted with a fluence of 5×10^{15} B$^+$ cm^{-2}. The reference sample shows the typical course. The measured S parameter in the damaged layer for implanted samples is clearly larger than the bulk S parameter due to positron trapping at ion-induced open-volume defects (see also the discussion in Sec. IV A 1 and Fig. 2). The relevant point in this experiment is that the data do not differ more than the experimental errors at the different directions for the same fluence. This means that the defect density and defect type of open-volume defects are equal too and are independent of substrate direction. In contrast, by using RBS different results are found for the various low-index directions. For an ion fluence of 5×10^{15} cm^{-2}, the relative concentration of displaced lattice atoms (n_{DA}) is plotted versus depth in Fig. 9 and the corresponding mean displacement distances r_a (perpendicular to the axis of incidence) are given. As can be seen, different values are obtained for ⟨100⟩, ⟨110⟩, and ⟨111⟩ oriented Si. The samples were implanted in one run and, in order to avoid channeling effects, implantation was performed in a 7° off-axis direction. Therefore, it can be assumed that the same amount of damage is produced independently of the substrate orientation. This assumption is confirmed by VEPAS, which gives almost identical $S(E)$ curves for all Si substrates investigated (see Fig. 8). That means that the differences observed by RBS (Fig. 9) have to be connected to an anisotropic lattice distortion caused by the implantation-induced defects. It should be mentioned that the determined displacement distance is a mean value comprising both large values that represent the defect complexes and low values that arise from the lattice distortion in the surrounding of the defect complexes. Consequently, n_{DA} is the concentration of all displaced lattice atoms and not the concentration of defects. Therefore, the results plotted in Fig. 9 indicate that in the ⟨100⟩ direction pronounced lattice distortions occur, i.e., low r_a and large concentration are observed, whereas in the ⟨110⟩ and ⟨111⟩ directions heavily displaced atoms are dominant. Comparing the depth distribution of defects determined by RBS (Fig. 9) to that obtained with the help of VEPAS (Fig. 3), it follows that the latter one extends to larger depth. This is a consequence of the higher sensitivity of VEPAS, which allows the detection of open-volume defects up to relative concentrations of less than 5%, which is not the case for RBS.

B. Annealing experiments

In electron-irradiated samples only monovacancies, divacancies, and vacancy impurity complexes were found.[31] The primary irradiation defects are close Frenkel pairs. The simple model is that new defects are formed when monovacancies become mobile around 100 K. The annealing characteristics in silicon is strongly influenced by the impurity content and additionally by the charge states of the defects. However, the divacancies anneal between 400 and 650 K.[31–33]

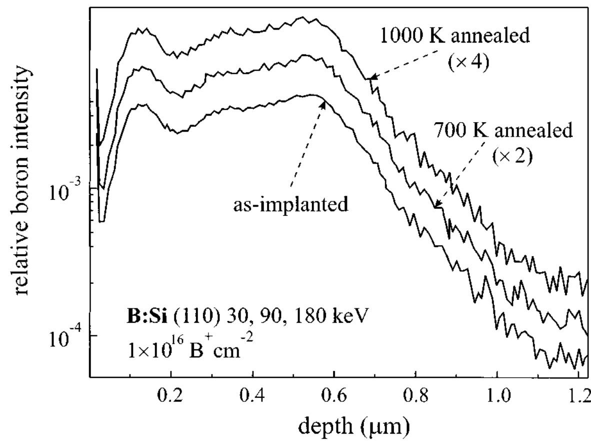

FIG. 10. Boron SNMS profiles of boron-implanted silicon samples in the as-implanted state and annealed (700 and 1000 K). The curves were almost identical and are shifted by a factor of 2 for clarity.

Defect reactions lead to different defect types appearing during the temperature treatment of ion-implanted samples too. The annealing behavior also depends on implantation fluence and sample material. First, we show the SNMS data to extract the behavior of implanted boron during sample annealing. The SNMS profiles of the $1\times10^{16}\ B^{+}\ cm^{-2}$ implanted sample annealed at different temperatures are presented in Fig. 10 as an example. The profile shows clearly the three-boron maxima caused by the multiple implantation mode. Furthermore, the boron profiles are not changed during annealing at different temperatures (up to 1000 K) significantly, i.e., boron profiles are completely identical after annealing at 700 and 1000 K. Hence boron diffusion can be neglected up to 1000 K.

1. Dependence of annealing behavior on oxygen concentration in sample material

Two different technologies are used for silicon single-crystal growth (encapsulated Czochralski and floating zone). The most important difference between the grown single crystals is the oxygen concentration of about $10^{18}\ cm^{-3}$ in Czochralski material and about $10^{16}\ cm^{-3}$ in FZ material. The differences of the annealing behavior for boron-implanted ($1\times10^{14}\ B^{+}\ cm^{-2}$) Czochralski Si and FZ Si are presented in Fig. 11. The S curves of the as-implanted state (300 K) show the typical course for both samples. The thin oxide film at the surface produces a low S parameter, the damaged layer causes a high S parameter, and at high positron energies the S parameter is characteristic for bulk material. The surface S parameter is shifted to a larger value at about 500 K. No distinct qualitative change in the bulk was found in positron measurements up to 650 K. The main annealing stage was observed at a temperature of about 720 K. After this stage, the S parameter of the disordered layer in Czochralski material decreases to a lower value than the bulk S parameter. In contrast, the FZ sample exhibits no significant decrease below the bulk S parameter. This fact is shown in Fig. 12, where the S parameter is plotted versus annealing temperature. The S parameter data in a depth range 100–300 nm were averaged to reduce data scattering. The discussion

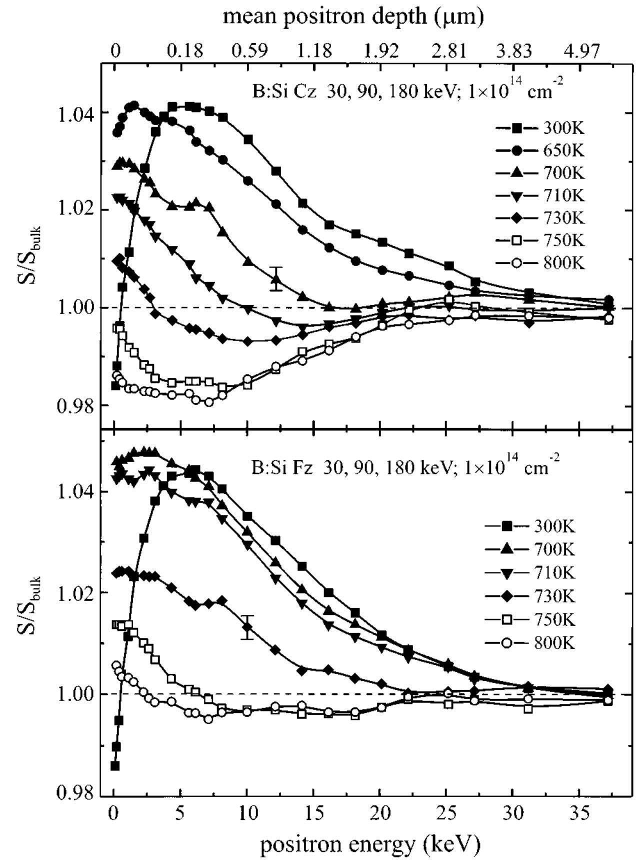

FIG. 11. Comparison of S parameter curves for FZ and Czochralski Si during isochronal annealing. Both samples were P doped and implanted with $1\times10^{14}\ B^{+}\ cm^{-2}$. The lines are only a guide for the eye.

of Fig. 12 is rather complex since defect annealing and the formation of new defects are obviously superimposed in Czochralski material, i.e., the measured S parameter is a mixed value. Nielsen *et al.* observed the same different behavior for Czochralski and FZ Si implanted with 5-MeV silicon ions.[28] The defects visible at 800 K indicated by a lower S parameter in Czochralski material are apparently related to oxygen impurities[34] and to the defects produced

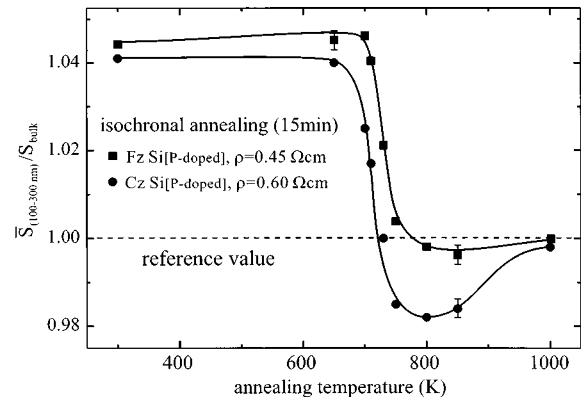

FIG. 12. Annealing stages of FZ and Czochralski material shown as the temperature dependence of the mean S parameter of a depth range 100–300 nm. The lines are only a guide for the eye.

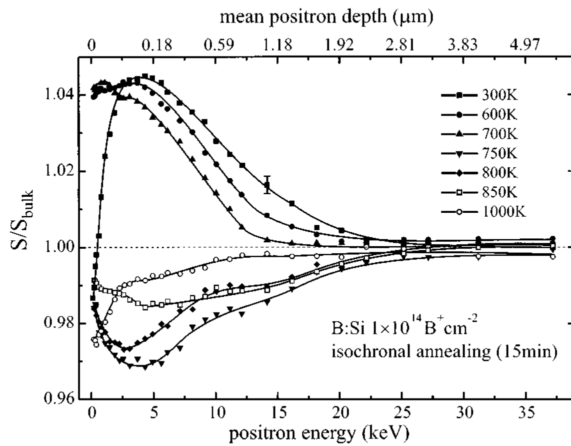

FIG. 13. Annealing behavior of 1×10^{14} B$^+$ cm^{-2} Czochralski Si shown by S parameter curves.

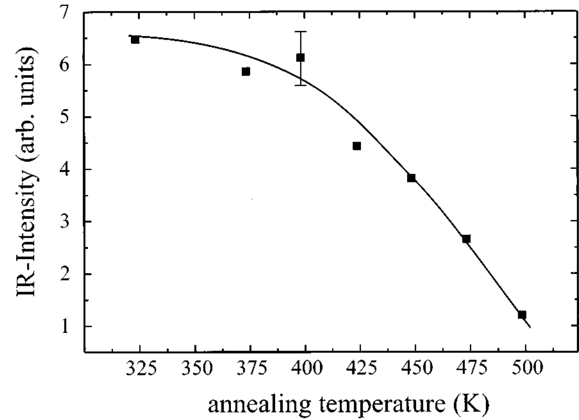

FIG. 15. Annealing stage of divacancies in Czochralski Si after implantation with 1×10^{14} B$^+$ cm^{-2} measured by IR absorption. The lines are only a guide for the eye.

during ion implantation. They are stable up to 900 K. The exact nature of this defect complex is unknown, but several properties can be extracted. The necessary presence of oxygen implies that the observed defect complexes contain oxygen atoms. Since the complex is a positron trap at elevated temperatures, it must include at least one vacancy. The simple VO complex can be excluded since it is only stable up to 600 K.[35] Hence it must be a larger complex consisting of vacancies and oxygen atoms; e.g., Lee *et al.* found that especially the V_3O_3 is stable up to 870 K.[36] Furthermore, it cannot be excluded that this complex exists prior to the main implantation defect is annealed. At lower annealing temperatures, the positron trapping in the main defect dominates and the oxygen-vacancy complex could be hidden. The signal of the V_xO_y complex is much smaller in FZ material due to the reduced oxygen concentration. Thus the main annealing stage can be studied almost independently of these oxygen-vacancy complexes.

2. Dependence of annealing behavior on boron fluence

The dependence of the annealing behavior on boron fluence was studied in Czochralski material (Figs. 13 and 14). As expected, the sample implanted with a fluence of 1

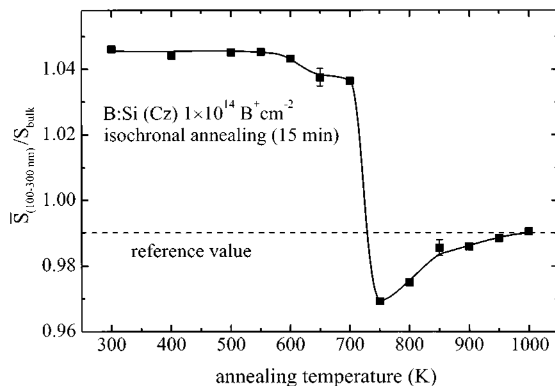

FIG. 14. Annealing behavior of 1×10^{14} B$^+$ cm^{-2} Czochralski Si characterized by the S parameter obtained by averaging the S values in the depth range 100–300 nm. The lines are only a guide for the eye.

$\times10^{14}$ B$^+$ cm^{-2} behaves similarly to the Czochralski sample in the previous experiment. The main annealing stage at 720 K is attributed to small vacancy clusters. Uedono *et al.* have found an annealing temperature of 1000 K for vacancy clusters.[37] However, these clusters should be larger than four vacancies. Additionally, a weak decrease of the S parameter is observed for the three annealings 600, 650, and 700 K (Fig. 14). In a superficial consideration one could attribute this stage to the divacancy annealing that occurs between 450 and 620 K.[32,38] This annealing was observed by the vanished intensity of the 0.68-eV band in IR absorption spectra (see Fig. 15). Here the annealing temperature was determined to be 470 K; which is in good agreement with the values in the literature.[32] However, the annealing of the divacancies has no noticeable influence on the S parameter. On the other hand, the formation of the oxygen-vacancy complex discussed above would explain the observed S parameter decrease between 550 and 650 K.

The annealing behavior of the highly implanted (1×10^{16} B$^+$ cm^{-2}) sample is different from the low-dose implanted sample in one feature. A new S parameter component becomes visible in a temperature range from 700 to 850 K and at positron energies between 1 and 3 keV (Fig. 16). This behavior can be attributed to the formation of a different defect type in the near-surface region that appears only at high boron fluences. Here the S parameter increases above S_{cl}, which is visible at room temperature after annealing at 700 K. It is obvious that a different defect is formed close to the surface that is different from the primarily introduced defect clusters. The high-S parameter implies the formation of larger vacancy clusters. On the other hand, a higher S can also be caused by a change in the chemical environment, i.e., it could be attributed to boron-related defects. At this sample, the concentration of the implanted boron should be larger as the equilibrium solid solubility.[39] However, SNMS measurements showed that the boron distribution was not influenced by annealing. A distinct defect diffusion happened at temperatures below 725 K, as can be seen from the narrowing of the $S(E)$ curve. Thus the agglomeration of defect clusters seems to be a more probable explanation for our results.

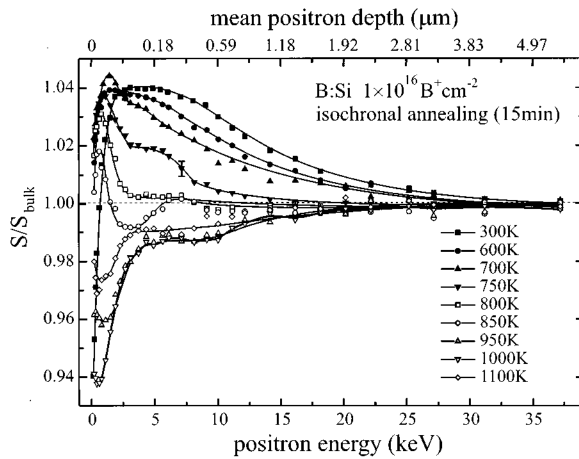

FIG. 16. Annealing behavior of 1×10^{16} B^{+} cm^{-2} Czochralski Si shown by S parameter curves. The lines are only a guide for the eye.

V. CONCLUSION

Defects and defect reactions were studied in boron-implanted silicon samples and during annealing treatment by slow positrons, RBS, SNMS, and IRAS measurements. The following conclusions were drawn.

(i) There is no amorphization of the silicon target by boron implantation at room temperature up to fluences of 2×10^{16} B^{+} cm^{-2}. The RBS data show a clear difference from a random spectrum, which is typical for amorphous layers.

(ii) A nearly constant divacancy signal was detected by IR absorption in a wide fluence range (1×10^{14} to 2×10^{16} $B^{+}cm^{-2}$), whereas an increase of the integral defect concentration obtained by slow positrons and RBS is proportional to the square root of the fluence, which is in accordance with the model of homogeneous defect nucleation.

(iii) We conclude that beside divacancies, larger vacancy clusters (containing three or four vacancies) exist in the as-implanted state. The S parameter of this defect was determined to be $S_{\rm cl}/S_{\rm bulk}=1.048\pm0.001$. This assumption is further supported by the thermal stability of these defects. The main annealing stage was found at 720 K, whereas the annealing of divacancies occurs at 470 K.

(iv) A distinguished dependence of atomic displacements on implantation direction was found in the RBS experiment, while the vacancylike defects detected by slow positrons do not show such a dependence. This means that the RBS data show an anisotropic lattice distortion caused by the implantation-induced defects.

(v) The different oxygen concentration in Czochralski (10^{13} cm^{-3}) and floating zone silicon (10^{16} cm^{-3}) has an influence on the defect reaction occurring during the annealing. In contrast to FZ material, in Czochralski silicon a positron trap was detected in the temperature range between 750 and 900 K, which exhibits an S parameter lower than the bulk S parameter. It was concluded that its nature is a complex consisting of at least a vacancy and an oxygen atom. Due to its thermal stability up to 600 K, the simple V-O complex must be excluded.

(vi) For the highly implanted (1×10^{16} $B^{+}cm^{-2}$) sample a different defect type was created in a 100-nm layer behind the surface due to heating at 700 K. This defect is stable up to 850 K. It is possible that larger vacancy clusters or boron-stabilized open-volume defects were generated due to agglomeration of mobile open-volume defects.

ACKNOWLEDGMENTS

The authors would like to thank B. Müller (TU Berlin) and G. Lenk (FSU Jena) for performing the boron implantations. The IR measurements were supported by Dr. H. Riede (Uni Leipzig). Furthermore, we acknowledge the WACKER SILTRONIC GmbH for providing us with the silicon wafer material. This work was supported by the Deutsche Forschungsgemeinschaft.

[1] J. W. Mayer, L. Eriksson, S. T. Picraux, and J. A. Davies, Can. J. Phys. **46**, 663 (1968).
[2] P. Asoka-Kumar, K. G. Lynn, and D. O. Welch, J. Appl. Phys. **76**, 4935 (1994).
[3] J. Lindhard, J. Scharff, and H. Schiøtt, K. Dan. Vidensk. Selsk. Mat. Fys. Medd. **33**, 1 (1963).
[4] W. Eckstein, *Computer Simulation of Ion-Solid Interactions* (Springer-Verlag, Berlin, 1991).
[5] H. Ryssel and I. Ruge, *Ionenimplantation* (Teubner, Stuttgart, 1978).
[6] P. J. Schultz and K. G. Lynn, Rev. Mod. Phys. **60**, 701 (1988).
[7] K. Gärtner, K. Hehl, and G. Schlotzhauer, Nucl. Instrum. Methods Phys. Res. **216**, 275 (1983).
[8] K. Gärtner, K. Hehl, and G. Schlotzhauer, Nucl. Instrum. Methods Phys. Res. B **4**, 55 (1984); **4**, 63 (1984).
[9] E. Wendler, K. Gärtner, W. Wesch, U. Zammit, and K. N. Madhusoodanan, Nucl. Instrum. Methods Phys. Res. B **85**, 528 (1994).
[10] H. J. Stein, F. L. Vook, D. K. Brice, J. A. Borders, and S. T. Picraux, Radiat. Eff. **6**, 19 (1970).
[11] S. Valkealathi and R. M. Niemienen, Appl. Phys. A **35**, 51 (1984).
[12] V. J. Ghosh, Appl. Surf. Sci. **85**, 187 (1995).
[13] J. Gebauer, S. Eichler, R. Krause-Rehberg, and H. P. Zeindl, Appl. Surf. Sci. (to be published).
[14] J. Mäkinen, C. Corbel, P. Hautojärvi, and D. Mathiot, Phys. Rev. B **43**, 12 114 (1991).
[15] A. van Veen, H. Schut, J. de Vries, R. A. Hakvoort, and M. R. Ijpma, in *Positron Beams for Solids and Surfaces*, edited by Peter J. Schultz, Guiti R. Massoumi, and Peter J. Simpson, AIP Conf. Proc. No. 218 (AIP, New York, 1990), p. 171.
[16] S. Mantl and W. Triftshäuser, Phys. Rev. B **17**, 1645 (1978).
[17] L. Liszkay, C. Corbel, L. Baroux, P. Hautojärvi, M. Bayhan, A. W. Brinkmann, and S. Tatarenko, Appl. Phys. Lett. **64**, 1380 (1994).
[18] A. Uedono, S. Tanigawa, K. Suzuki, and K. Watanabe, Appl. Phys. Lett. **53**, 473 (1988).
[19] A. Kawasuso, M. Hasegawa, M. Suezawa, S. Yamaguchi, and K. Sumino, Jpn. J. Appl. Phys. 1 **34**, 2197 (1995).
[20] R. M. Nieminen and J. Laakkonen, Appl. Phys. **20**, 181 (1979).

[21] A. Uedono, S. Tanigawa, J. Sugiura, and M. Ogasawara, Appl. Phys. Lett. **53**, 25 (1988).
[22] L. Sealy, R. C. Barklie, G. Lulli, R. Nipoti, R. Balboni, S. Milita, and M. Servidori, Nucl. Instrum. Methods Phys. Res. B **96**, 215 (1995).
[23] L. T. Chadderton, Radiat. Eff. **8**, 77 (1971).
[24] U. Zammit, K. N. Madhusoodanan, M. Marinelli, F. Scudieri, R. Pizzoferrato, F. Mercuri, E. Wendler, and W. Wesch, Phys. Rev. B **49**, 14 322 (1994).
[25] R. D. Goldberg, P. J. Schultz, and P. J. Simpson, Appl. Surf. Sci. **85**, 287 (1995).
[26] J. Keinonen, M. Hautala, E. Rauhala, V. Karttunen, A. Kuronen, E. Rauhala, A. Vehanen, E. Punkka, and P. Hautojärvi, Phys. Rev. B **37**, 8269 (1988).
[27] P. J. Simpson, Appl. Surf. Sci. (to be published).
[28] B. Nielsen, O. W. Holland, T. C. Leung, and K. G. Lynn, J. Appl. Phys. **74**, 1636 (1993).
[29] K. L. Brower, Radiat. Eff. **8**, 213 (1971).
[30] K. L. Brower and W. Beezhold, J. Appl. Phys. **43**, 3499 (1972).
[31] J. Bourgoin and M. Lannoo, in *Point Defects in Semiconductors II, Experimental Aspects*, edited by M. Cardona, Springer Series in Solid-State Sciences Vol. 35 (Springer-Verlag, Berlin, 1983).
[32] L. J. Cheng, J. Corelli, J. W. Corbett, and G. D. Watkins, Phys. Rev. B **152**, 761 (1966).
[33] L. J. Cheng and J. Lori, Phys. Rev. B **171**, 171 (1968).
[34] S. Dannefaer and J. Kerr, J. Appl. Phys. **60**, 1313 (1986).
[35] A. Uedono, L. Wei, C. Dosho, Y. Tabuki, H. Kondo, S. Tanigawa, and M. Tamura, Mater. Sci. Forum **105-110**, 1471 (1992).
[36] Y. H. Lee and J. W. Corbett, Phys. Rev. B **13**, 2653 (1976).
[37] A. Uedono, L. Wei, and S. Tanigawa, Radiat. Eff. Defects Solids **124**, 31 (1992).
[38] A. Kawasuso, M. Hasegawa, M. Suezawa, S. Yamaguchi, and K. Sumino, Hyperfine Interact. **84**, 397 (1994).
[39] R. B. Fair, in *Semiconductor Silicon*, edited by H. R. Huft and E. Sintl (Electrochemical Society, New York, 1977), p. 968.
[40] P. J. Simpson, M. Vos, I. V. Mitchell, C. Wu, and P. J. Schultz, Phys. Rev. B **44**, 12 180 (1991).